Supplementary Materials

Hydrogel-Based Biocontainment of Bacteria for Continuous Sensing and Computation

Tzu-Chieh Tang[1,2,3,17,*], Eléonore Tham[1,4,17], Xinyue Liu[5,17], Kevin Yehl[1,2,13], Alexis J. Rovner[6,7], Hyunwoo Yuk[5], Cesar de la Fuente-Nunez[1,2,14,15,16], Farren J. Isaacs[8,9,10], Xuanhe Zhao[5,11,*], Timothy K. Lu[1,2,12,*]

[1]Synthetic Biology Group, Research Laboratory of Electronics, Massachusetts Institute of Technology, Cambridge, MA 02139, USA.
[2]Department of Biological Engineering, Massachusetts Institute of Technology, Cambridge, MA 02139, USA.
[3]The Mediated Matter Group, Media Lab, Massachusetts Institute of Technology, Cambridge, MA 02139, USA
[4]Department of Materials Science and Engineering, Massachusetts Institute of Technology, Cambridge, MA 02139, USA.
[5]Department of Mechanical Engineering, Massachusetts Institute of Technology, Cambridge, MA 02139, USA.
[6]Wyss Institute for Biologically Inspired Engineering, Boston, MA 02115, USA.
[7]Department of Genetics, Harvard Medical School, Harvard University, Boston, MA 02115, USA.
[8]Department of Molecular, Cellular and Developmental Biology, Yale University, New Haven, CT 06520, USA.
[9]Systems Biology Institute, Yale University, West Haven, CT 06516, USA.
[10]Department of Biomedical Engineering, Yale University, New Haven, CT 06520, USA
[11]Department of Civil and Environmental Engineering, Massachusetts Institute of Technology, Cambridge, MA 02139, USA
[12]Department of Electrical Engineering and Computer Science, Massachusetts Institute of Technology, Cambridge, MA 02139, USA.
[13]Present address: Department of Chemistry and Biochemistry, Miami University, Oxford, OH 45056, USA.
[14]Present address: Machine Biology Group, Departments of Psychiatry and Microbiology, Institute for Biomedical Informatics, Institute for Translational Medicine and Therapeutics, Perelman School of Medicine, University of Pennsylvania, Philadelphia, PA 19104, USA.
[15]Present address: Departments of Bioengineering and Chemical and Biomolecular Engineering, School of Engineering and Applied Science, University of Pennsylvania, Philadelphia, PA 19104, USA.
[16]Present address: Penn Institute for Computational Science, University of Pennsylvania, Philadelphia, PA 19104, USA.

[17]T.-C.T., E.T., and X.L. contributed equally to this work.

[*]Correspondence and requests of materials should be addressed to T.-C.T. (zijaytang@gmail.com), X.Z. (zhaox@mit.edu), and T.K.L. (timlu@mit.edu).

Supplementary Tables & Figures

Supplementary Table 1 | List of bacterial strains used in this study

Name	Strain code	Construction method	Genotype	Used in
GRO, pIF auxotroph strain	rEc.β.dC.12'.ΔtY	Ref[1]	MG1655	Fig. 4
GRO, pIF auxotroph strain	LspA.Y54β	Ref[1]	MG1655	Fig. 4
aTc sensing strain	EZ055	DH5αPRO cells transformed with the pEZ055 plasmid	DH5αPRO	Fig. 3 Fig. 5
F' plasmid donor strain	CJ236	Acquired from NEB	K12	Fig. 4
F' plasmid recipient strain	rcF453	Spontaneous resistant mutants generated from plating and re-streaking MG1655 on LB+Sm plate	MG1655	Fig. 4
Zn/Pb/Cd sensing strain	EZ074	DH5αPRO cells transformed with the pEZ074 plasmid	DH5αPRO	Fig. 5
SCRIBE $kanR_{OFF}$ reporter strain	F144	Ref[2]	DH5αPRO $galK::kanR_{W28TAA,\ A29TAG}$	Fig. 5
AHL sender strain	AYC261	Ref[3]	DH5αPRO	Fig. 5
AHL receiver strain	EZ058	DH5αPRO cells transformed with the pEZ058 plasmid	DH5αPRO	Fig. 5
Heme sensing strain	mm1560	Ref[4]	Nissle 1917	Fig. 5

Supplementary Table 2 | List of plasmids used in this study

Name	Plasmid code	Construction method	Used in
$P_{LtetO-1}$_*gfp*	pEZ055	See Methods and Supplementary Fig. 17	Fig. 5
P_{lux}_*gfp*	pEZ058	See Methods and Supplementary Fig. 17	Fig. 5
P_{zntA}_*gfp*	pEZ074	See Methods and Supplementary Fig. 17	Fig. 5
P_{lacO}_SCRIBE(*kanR*)on	F944	Ref[2]	Fig. 5
P_{TetO}_CRISPRi(*recJ*_gRNA & *xonA* gRNA)	F1156	Ref[5]	Fig. 5
P_{TetO}_*LuxI*	AYC261	Ref[3]	Fig. 5

Supplementary Fig. 1

Supplementary Fig. 1 | Alginate cores in various geometries. The alginate core used to encapsulate cells can be shaped into spheres with different radii through extrusion with syringes and needles on parafilm followed by crosslinking in calcium chloride solution. Alginate thread was produced by direct extrusion in calcium chloride solution. Disk, cube, and cylinder-like structures can be achieved through cutting.

Supplementary Fig. 2

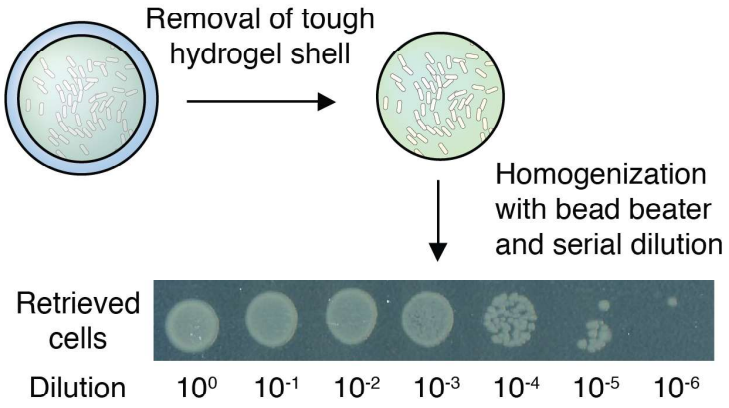

Supplementary Fig. 2 | Retrieving encapsulated cells. Retrieval of live cells from the beads immediately before the cross-linking step. Retrieval was performed through removal of the tough shell followed by homogenization and showed nearly full recovery (~10^9 CFU per mL).

Supplementary Fig. 3

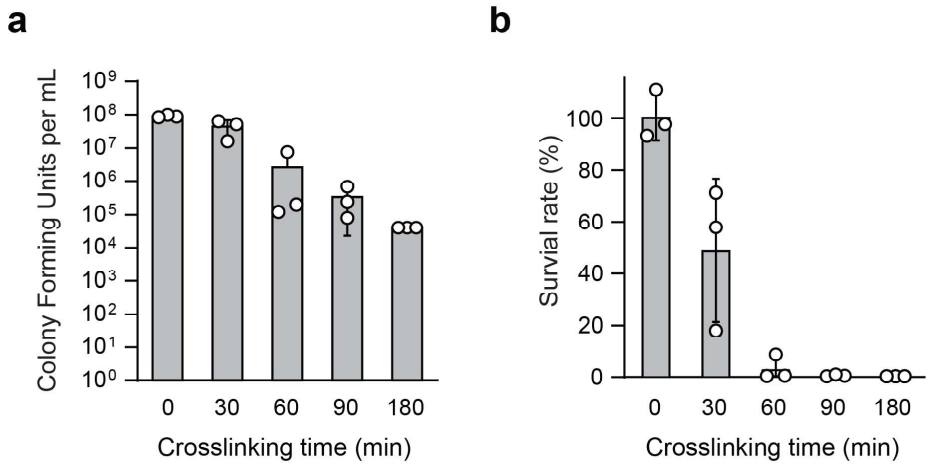

Supplementary Fig. 3 | Toxicity of the chemical crosslinkers. (a) CFU counts and **(b)** survival rates for cells retrieved from hydrogel beads after incubating in the crosslinking solution for different lengths of time. Samples prepared in triplicate, data represent the mean ±1 SD.

Supplementary Fig. 4

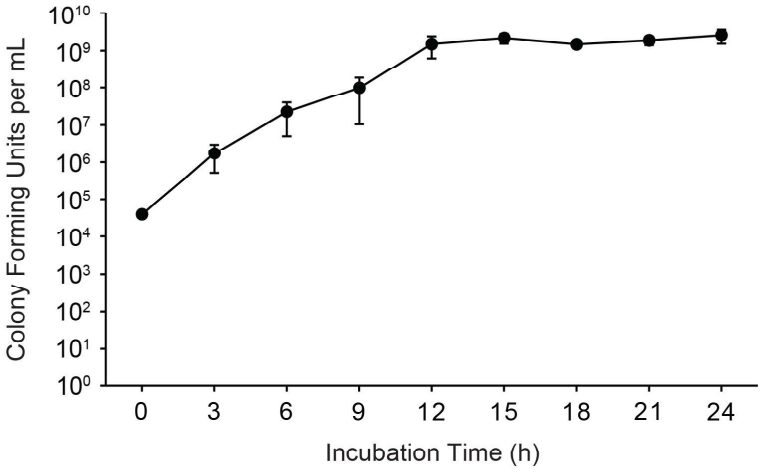

Supplementary Fig. 4 | Growth curve of bacteria in hydrogel beads. Cell encapsulated in beads were incubated in LB medium and retrieved at given time points to measure growth over 24 hours. Samples prepared in triplicate, data represent the mean ±1 SD.

Supplementary Fig. 5

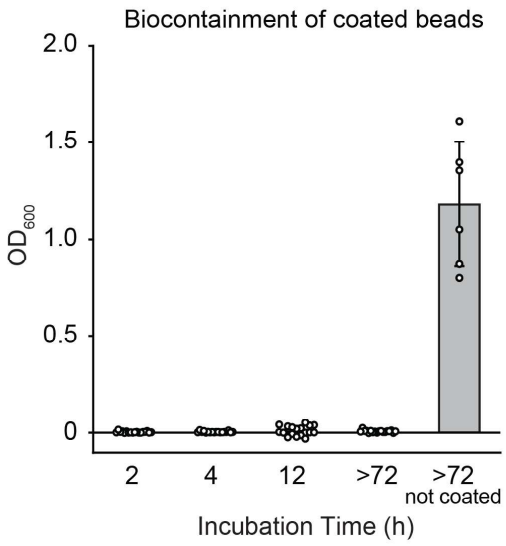

Supplementary Fig. 5 | Long-term physical containment. Optical density at 600 nm (OD_{600}) measurement demonstrating that the media surrounding coated beads showed no bacterial growth after 72 hours. Samples prepared in n = 18 coated beads for h = 2, 4, 12, and >72, and n = 6 beads that are not coated. Data represent the mean ±1 SD.

Supplementary Fig. 6

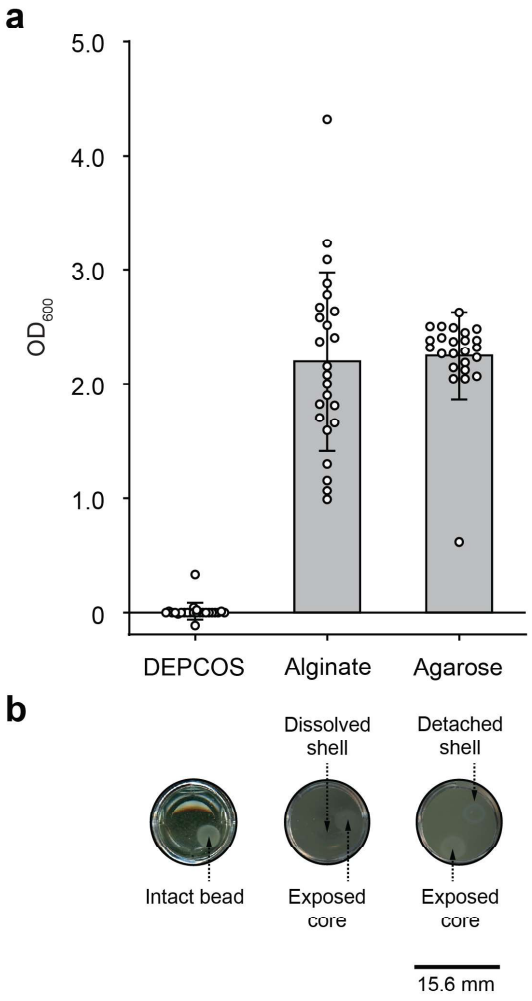

Supplementary Fig. 6 | Physical containment under prolonged shaking. (a) OD_{600} measurement demonstrating the bacterial growth in the media surrounding the beads after 12 hours of shaking at 200 rpm. Samples prepared in n = 24 beads, data represent the mean ±1 SD. **(b)** Representative images of the beads and their surrounding media after shaking. The DEPCOS beads (left) remained intact and showed no signs of cell leakage (clear media). The shell of the alginate-coated beads (center) was dissolved after prolonged shaking and could not stop the core from exposing. Similarly, the shell of the agarose-coated beads broke and detached from the core, leaving it exposed and causing cell escape.

Supplementary Fig. 7

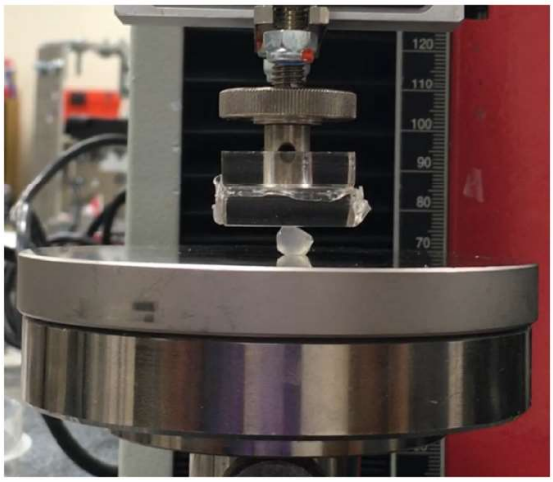

Supplementary Fig. 7 | Compression test setup with Zwick mechanical tester. A fully-hydrated hydrogel bead (r = 3 mm) was placed between sterile surfaces and submitted to compressions.

Supplementary Fig. 8

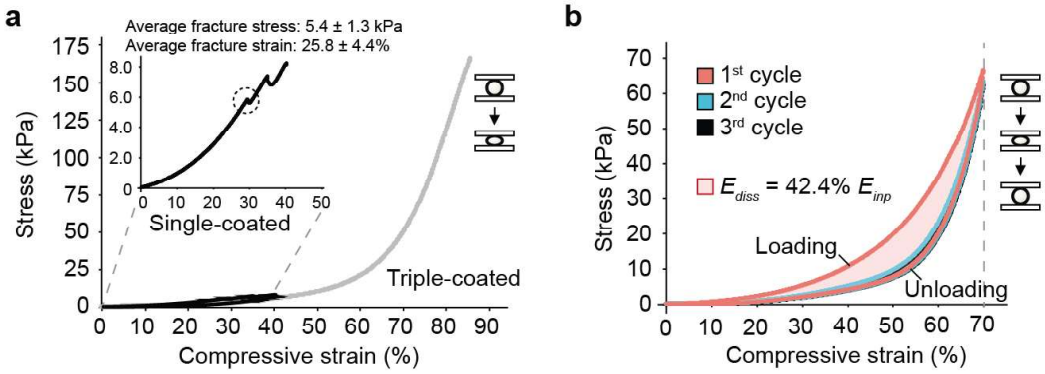

Supplementary Fig. 8 | Effective stress-strain profiles of the hydrogel beads under compression. (a) Effective stress-strain curves of single- and triple-coated beads. Samples prepared in n = 14 beads. **(b**) Effective stress-strain curves of cyclic compression of triple-coated beads. Effective stress-strain curves were converted from force-displacement curves using the initial dimensions of the beads before compressions[6,7]. Samples prepared in triplicate.

Supplementary Fig. 9

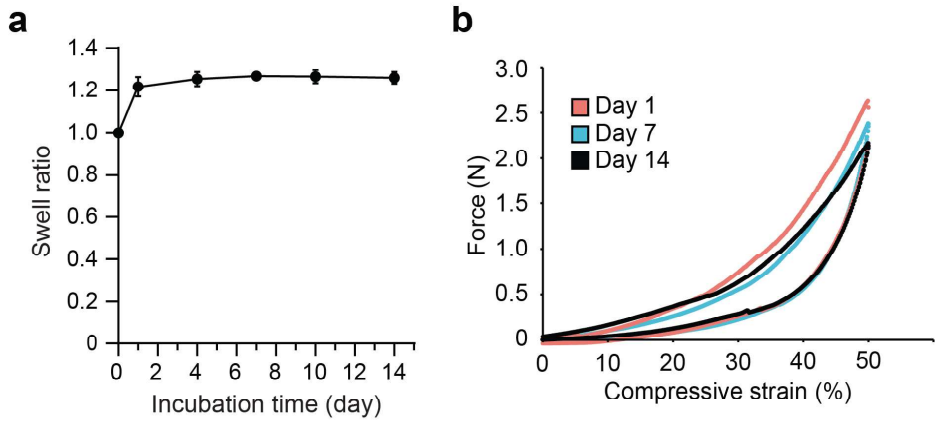

Supplementary Fig. 9 | Swelling and mechanical properties of the hydrogel beads after prolonged incubation. (a) The swelling behavior of beads over the course of 14 days. Samples prepared in *n* = 10 beads, data represent the mean ±1 SD. **(b**) Typical force-displacement curves of single-layer coated bead (r = 3 mm) on day 1, 7, and 14 of incubation.

Supplementary Fig. 10

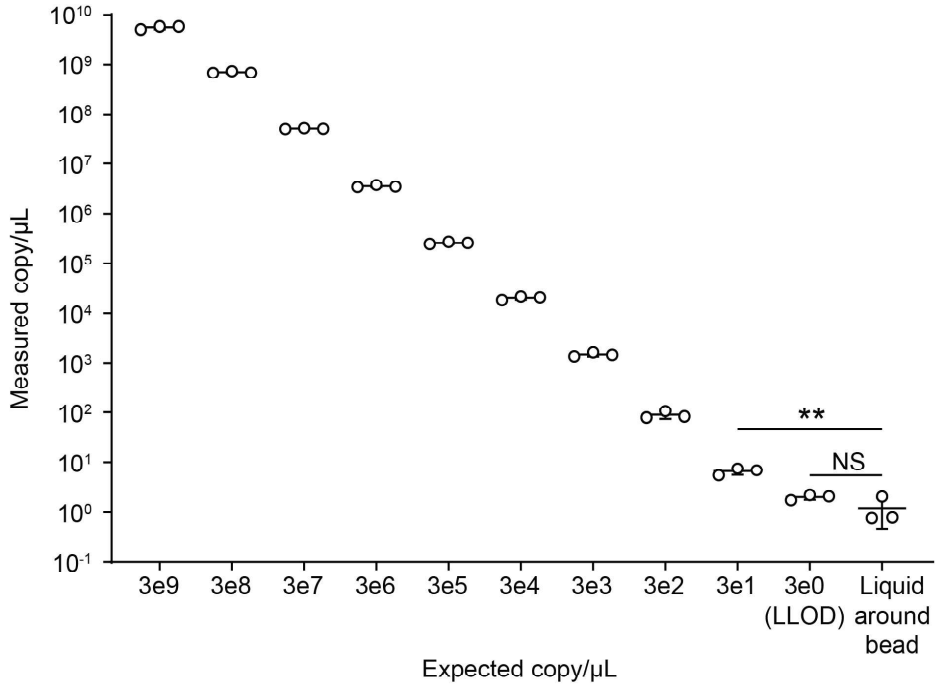

Supplementary Fig. 10 | DNA containment inside the hydrogel beads. Linear DNA fragments (977 bp) were PCR-amplified and encapsulated in the hydrogel beads at 3e9 copy/µL. Soluble DNA in the surrounding media after 72-hr incubation was quantified using qPCR. Standards were prepared by serial dilutions. Samples prepared in triplicate, data represent the mean ±1 SD. ***P* = 0.0018 (df = 4, 95% CI = -7.398 to -3.351), NS = not significant (*P* = 0.1460, df = 4, 95% CI =-2.035 to 0.4334). Statistics are derived using a two-tailed *t*-test. Lower limit of detection (LLOD) = 3 copy/µL.

Supplementary Fig. 11

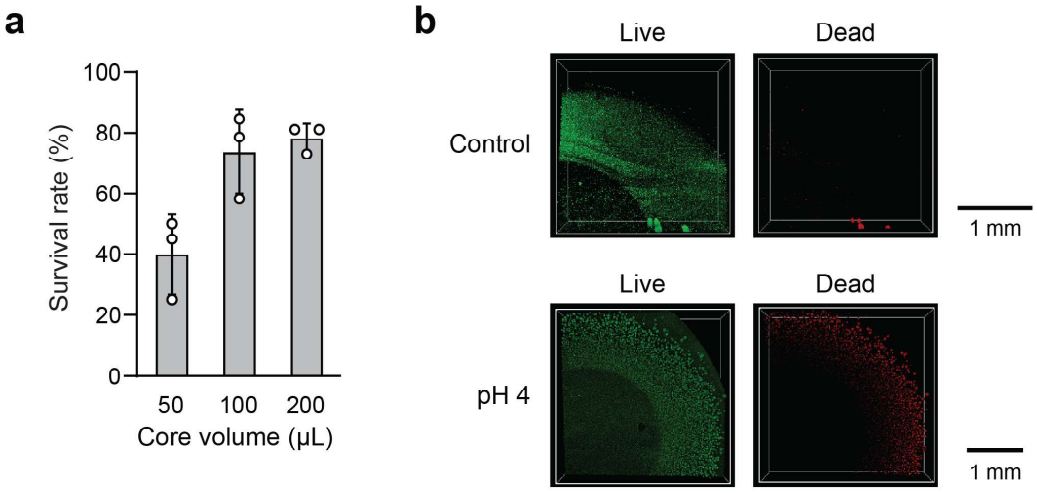

Supplementary Fig. 11 | Viability of encapsulated cells at pH 4. (a) Survival rates of cells encapsulated in alginate cores of different sizes after 4 hours of shaking incubation at pH 4. The final diameters of the beads after outgrowth are approximately 6 mm, 6.5 mm, and 8 mm for initial core volumes of 50 µL, 100 µL, and 200 µL, respectively. Data are calculated from triplicate incubated in original LB and LB adjusted to pH 4. Samples prepared in triplicate, data represent the mean ±1 SD. **(b)** Spatial distribution of live (green) and dead (red) cells in the 50 µL alginate cores after 4 hours of shaking incubation at pH 4. Depth of Z-stack is 580 µm for the control bead images and 800 µm for the pH 4 bead images. Images are representative of duplicates of similar results.

Supplementary Fig. 12

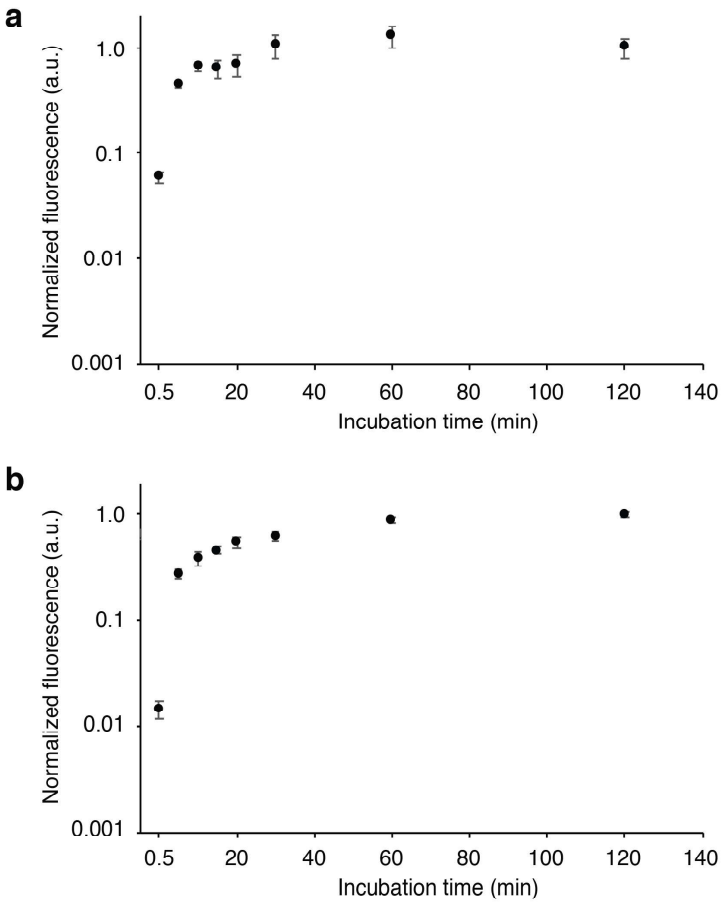

Supplementary Fig. 12 | Diffusion of small molecules into the hydrogel beads. (a) Diffusion of a positively charged dye, rhodamine, into the hydrogel beads over a course of two hours. **(b)** The diffusion profile of a negatively charged dye, fluorescein. Samples prepared in triplicate, data represent the mean ±1 SD.

Supplementary Fig. 13

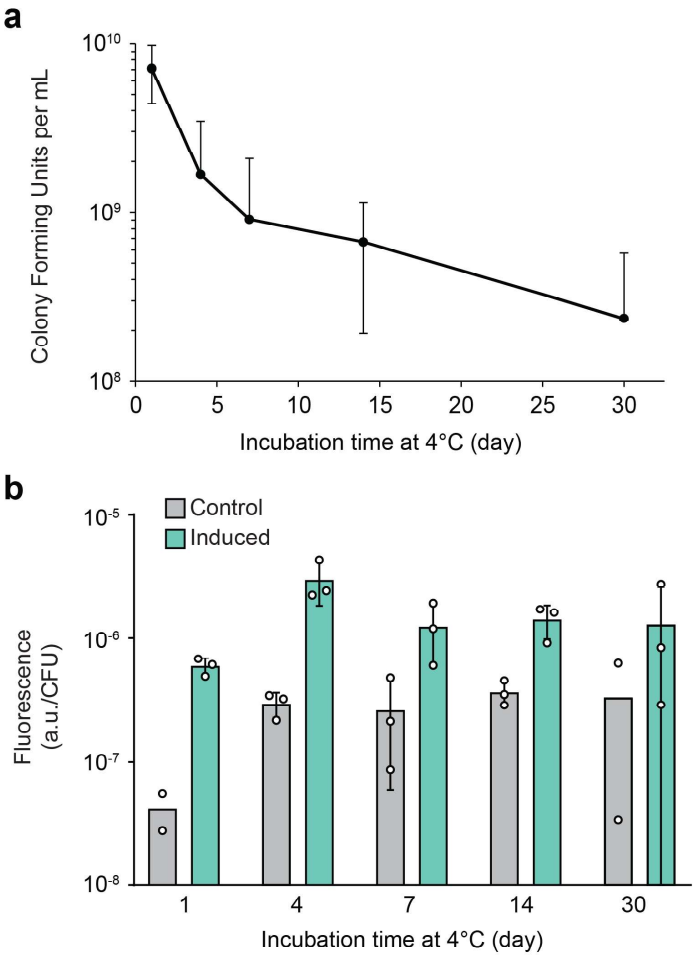

Supplementary Fig. 13 | Cell survival and inducibility after storage at low temperature. (a) CFU counts for cells retrieved from hydrogel beads after storage in a refrigerator (4°C) across 30 days **(B)** Comparison of aTc-induced fluorescence profiles of retrieved cells after storage at 4°C for various time periods. Samples prepared in triplicate (duplicate for the control group on day 1 and 30), data represent the mean ±1 SD.

Supplementary Fig. 14

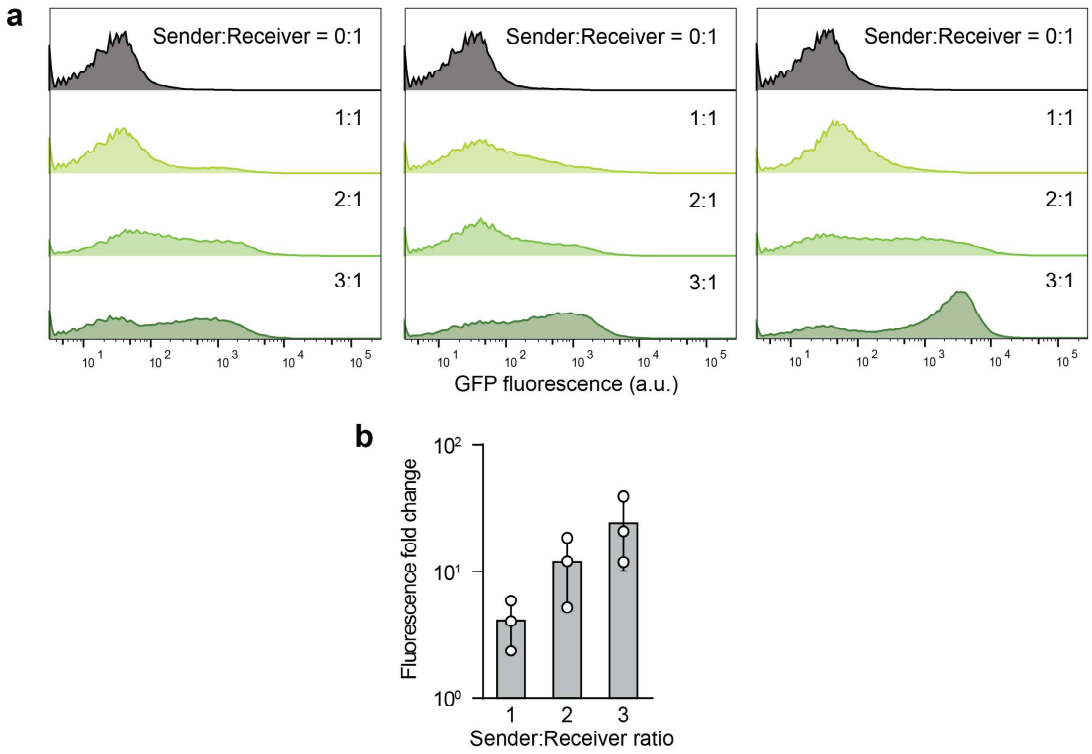

Supplementary Fig. 14 | Induction of AHL receiver beads by AHL sender beads. (a) Flow cytometry data of cells retrieved from receiver beads showed various levels of induction corresponding to different AHL sender bead to AHL receiver bead ratios (normalized to unit distribution, three biological replicates). **(b)** Fluorescence fold change of the receiver beads. Samples prepared in triplicate, data represent the mean ±1 SD.

Supplementary Fig. 15

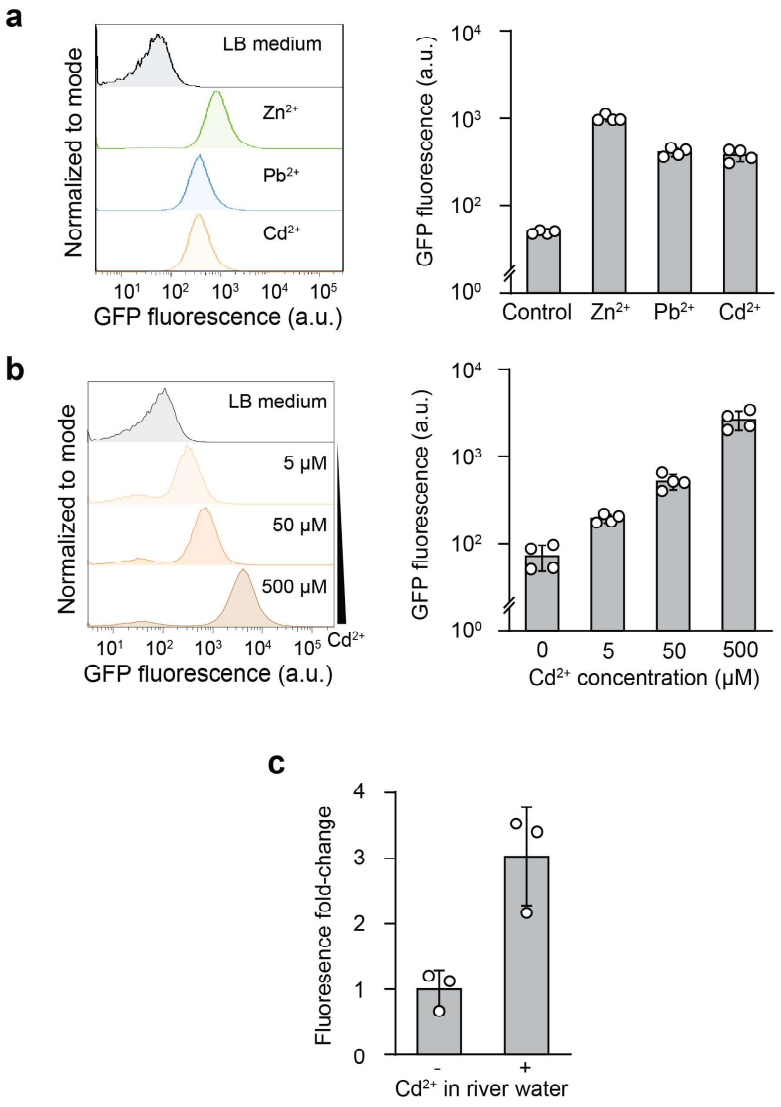

Supplementary Fig. 15 | Heavy metal sensing in Charles River water samples. (a) Left: Flow cytometry analysis of the heavy-metal-sensing strain. Bacteria in liquid were exposed for 3 hours to 300 μM $ZnCl_2$, 100 μM $Pb(NO_3)_2$, and 10 μM $CdCl_2$ in LB media, respectively. Right: Mean GFP fluorescence of the heavy-metal-sensing strain. Samples prepared in n = 4 beads for each condition, data represent the mean ±1 SD. **(b)** Left: Response of the heavy-metal-sensing strain encapsulated in the tough hydrogel capsule to 0 μM, 5 μM, 50 μM, and 500 μM $CdCl_2$ after 3 hours of incubation. Right: Mean GFP fluorescence of the heavy-metal-sensing strain encapsulated in the tough hydrogel capsule. Samples prepared in n = 4 beads, data represent the mean ±1 SD. **(c)** GFP fluorescence fold-change of encapsulated cells responding to cadmium ions in Charles River water. Samples prepared in n = 3 beads, data represent the mean ±1 SD.

Supplementary Fig. 16

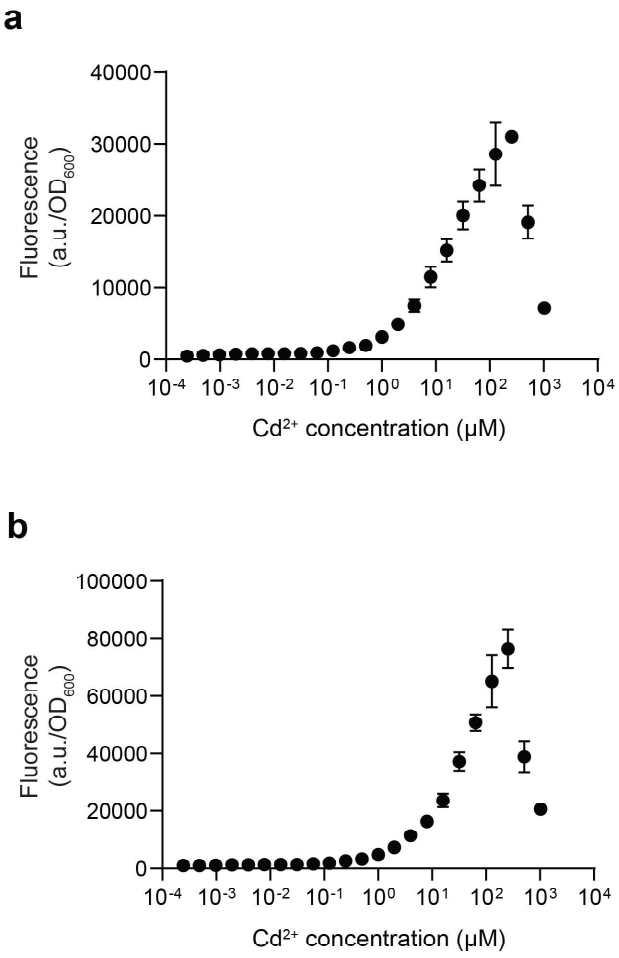

Supplementary Fig. 16 | Dose-response curves of P*zntA*-GFP induced by Cd^{2+}. The expression of GFP in cells harboring the plasmid pEZ074 after **(a)** 3 hours and **(b)** 6 hours of incubation with Cd^{2+}. Slow cell growth and reduced fluorescence were observed at [Cd^{2+}] > 256 μM. Samples prepared in triplicate, data represent the mean ±1 SD.

Supplementary Fig. 17

Supplementary Fig. 17 | Plasmid maps of pEZ055, pEZ058, and pEZ074. ColE1 rep: ColE1 origin of replication; amp marker: resistance gene cassette for carbenicillin; gfp: green fluorescence protein.

Supplementary Fig. 18

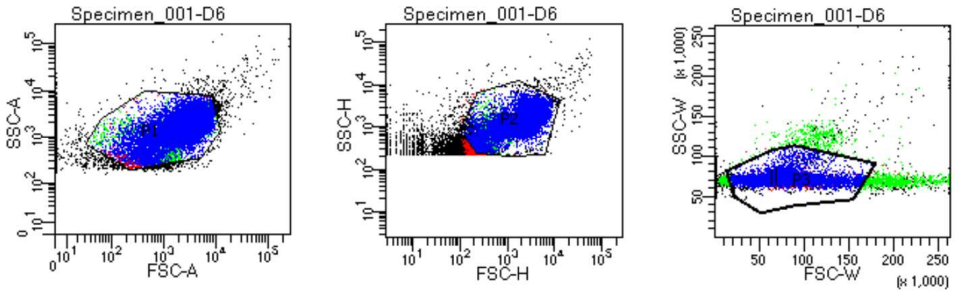

Population	#Events	%Parent	FITC-A Mean	FITC-A Median
All Events	33,967	####	1,103	634
P1	30,000	88.3	1,214	823
P2	29,693	99.0	1,227	841
P3	28,383	95.6	1,252	876

Supplementary Fig. 18 | Gating strategy for flow cytometry. Top: Cells were gated using log forward scatter area (FSC-A) by log side scatter area (SSC-A), followed by gating on log forward scatter height (FSC-H) by log side scatter height (SSC-H), and subsequent gating on log forward scatter width (FSC-W) by log side scatter width (SSC-W). Bottom: Cell population abundance during each gating stage, in numbers and percentages.

References

1. Rovner, A. *et al.* Recoded organisms engineered to depend on synthetic amino acids. *Nature* **518**, 89–93 (2015).
2. Farzadfard, F. & Lu, T. K. Genomically encoded analog memory with precise in vivo DNA writing in living cell populations. *Science (80-.).* **346**, 1256272–1256272 (2014).
3. Chen, A. Y. *et al.* Synthesis and patterning of tunable multiscale materials with engineered cells. *Nat. Mater.* **13**, 515–523 (2014).
4. Mimee, M. *et al.* An ingestible bacterial-electronic system to monitor gastrointestinal health. *Science (80-.).* **360**, 915–918 (2018).
5. Farzadfard, F. *et al.* Single-nucleotide-resolution computing and memory in living cells. *Mol. Cell* **75**, 769–780 (2019).
6. Tomović, N. S., Trifković, K. T., Rakin, M. P., Rakin, M. B. & Bugarski, B. M. Influence of compression speed and deformation percentage on mechanical properties of calcium alginate particles. *Chem. Ind. Chem. Eng. Q.* **21**, 411–417 (2015).
7. Liu, X. *et al.* Ingestible hydrogel device. *Nat. Commun.* **10**, 1–10 (2019).